

Published in final edited form as:

J Mol Biol. 2008 June 20; 379(5): 1075–1093. doi:10.1016/j.jmb.2008.04.044.

Hydrogen-Exchange Mass Spectrometry Reveals Activation-Induced Changes in the Conformational Mobility of p38 α MAP Kinase

Kevin M. Sours¹, Stan C. Kwok², Thami Rachidi^{1,†}, Thomas Lee^{1,‡}, Adam Ring¹, Andrew N. Hoofnagle^{1,§}, Katheryn A. Resing¹, and Natalie G. Ahn^{1,3,*}

C. R. Matthews

¹Department of Chemistry and Biochemistry, University of Colorado, Boulder, CO, USA

²Department of Biochemistry and Molecular Genetics, University of Colorado Health Sciences Center, Aurora, CO, USA

³HHMI, University of Colorado, Boulder, CO, USA

Abstract

Hydrogen–deuterium exchange measurements represent a powerful approach to investigating changes in conformation and conformational mobility in proteins. Here, we examine p38 α MAP kinase (MAPK) by hydrogen-exchange (HX) mass spectrometry to determine whether changes in conformational mobility may be induced by kinase phosphorylation and activation. Factors influencing sequence coverage in the HX mass spectrometry experiment, which show that varying sampling depths, instruments, and peptide search strategies yield the highest coverage of exchangeable amides, are examined. Patterns of regional deuteration in p38 α are consistent with tertiary structure and similar to deuteration patterns previously determined for extracellular-signal-regulated kinase (ERK) 2, indicating that MAPKs are conserved with respect to the extent of local amide HX. Activation of p38 α alters HX in five regions, which are interpreted by comparing X-ray structures of unphosphorylated p38 α and X-ray structures of phosphorylated p38 γ . Conformational differences account for altered HX within the activation lip, the P + 1 site, and the active site. In contrast, HX alterations are ascribed to activation-induced effects on conformational mobility, within substrate-docking sites (α F– α G, β 7– β 8), the C-terminal core (α E), and the N-terminal core region (β 4– β 5, α L16, α C). Activation also decreases HX in a 3–10 helix at the C-terminal extension of p38 α . Although this helix in ERK2 forms a dimerization interface that becomes protected from HX upon activation, analytical ultracentrifugation shows that this does not occur in p38 α because both unphosphorylated and diphosphorylated forms are monomeric. Finally, HX patterns in monophosphorylated p38 α are similar to those in unphosphorylated kinase, indicating that the major activation lip remodeling events occur only after diphosphorylation. Importantly, patterns of activation-induced HX show differences between p38 α and ERK2 despite their similarities in overall deuteration, suggesting that although MAPKs are closely related with respect to primary sequence and tertiary structure, they have distinct mechanisms for dynamic control of enzyme function.

© 2008 Elsevier Ltd. All rights reserved.

*Corresponding author. Natalie.Ahn@colorado.edu.

†Current address: T. Rachidi, Ingram Micro, Inc., 1600 East St. Andrew Place, Santa Ana, CA 92705, USA.

‡Current address: T. Lee, Department of Biochemistry, University of Wisconsin, Madison, WI 53706, USA.

§Current address: A. N. Hoofnagle, Department of Laboratory Medicine, School of Medicine, University of Washington, Seattle, WA 98195, USA.

Supplementary Data

Supplementary data associated with this article can be found, in the online version, at doi:10.1016/j.jmb.2008.04.044

Keywords

MAP kinase; p38; hydrogen exchange; mass spectrometry; conformational mobility

Introduction

MAP kinase (MAPK) family members, including various forms of extracellular-signal-regulated kinase (ERK), Jun N-terminal kinase (JNK), and p38 MAPK, control diverse aspects of cellular regulation. p38 MAPKs and JNKs regulate responses to stress and inflammation, while ERKs regulate events required for cell proliferation, motility, and differentiation. Many family members are under exploration as drug targets, and inhibitors of p38 show therapeutic effects towards diseases of inflammation.¹ MAPKs are closely related by sequence, with p38 α MAPK sharing 48% sequence identity with ERK2 and 60% identity with p38 β and p38 γ MAPK forms.

Mechanisms for activating MAPKs are conserved. Like other protein kinases, they display a conserved bilobed kinase structure, consisting of an active site located between an N-terminal ATP-binding domain and a C-terminal substrate-binding domain.² Each MAPK is activated by dual phosphorylation at a pThr-Xxx-pTyr sequence motif located within the activation lip. This leads to conformational changes around the active site, which are best understood for ERK2—the only MAPK for which X-ray structures of both inactive and active forms have been determined.^{3,4} Three major changes occur as a result of dual phosphorylation. First, ion pair interactions between the phosphorylated residues and basic side-chain amino acids cause a dramatic reorganization of the activation lip into a conformation that enables substrate binding and recognition of a Ser/Thr-Pro sequence motif for phosphorylation. Second, ion pair interactions lead to connectivity between the lip and the N-terminal helix α C, as well as repositioning of active-site residues for catalysis. Third, a docking motif-binding site forms upon reorganization of the activation lip, enabling high-affinity substrate binding.⁵ Thus, dual phosphorylation and activation lip remodeling lead to conformational changes that facilitate substrate binding and formation of a competent catalytic site.

In addition to conformational changes, protein kinase activation causes changes in internal protein motions as determined by hydrogen-exchange mass spectrometry (HX-MS).^{6,7} By examining HX with D₂O on peptides formed by proteolysis, localized effects within a molecule can be detected.^{8,9} Several studies have now shown that HX measurements on kinases detect localized changes in protein fluctuations that are low energy and not always observable by X-ray crystallography.^{7,10–12} These can include motional changes, in which a protein adopts conformers that differ by free energies on the order of 1 kcal/mol. Regulation of protein fluctuations and flexibility could lead to changes in protein function, even when structural changes are not apparent.

HX-MS measurements reveal that, in ERK2, kinase activation leads to changes in hydrogen–deuterium exchange at backbone amides within the hinge region separating N- and C-terminal domains.⁷ Because X-ray structures show that atoms within the hinge region are superimposable between active and inactive forms, the corresponding changes in HX have been ascribed to regulated conformational mobility. In agreement, site-directed spin labeling EPR measurements show activation-induced changes in correlation times of side chains at hinge residues.¹³ Furthermore, evidence from HX-MS suggests that regulated protein motions are important for activation. In the active form of ERK2, the nonhydrolyzable ATP analog, AMP-PNP, sterically protects amides from hydrogen–deuterium exchange in both the N-terminal and the C-terminal domains of the ATP-binding pocket.¹⁴ In contrast, only the N-terminal domain is protected from exchange by AMP-PNP in the inactive form of ERK2. This

indicates that, in solution, the N- and C-terminal lobes in active ERK2 adopt a closed conformation around nucleotides, whereas inactive ERK2 is somehow constrained from interdomain closure and instead adopts an open conformation. Together, the evidence suggests that increased backbone flexibility at the hinge following ERK2 phosphorylation enables induced-fit interdomain closure, a necessary event for catalytic function.

X-ray structures of p38 α MAPK and JNK1 in their inactive forms show a large diversity in activation lip conformation.^{15–19} Although structures of corresponding active forms are not available, an X-ray structure of diphosphorylated active p38 γ MAPK reveals that the activation lip adopts a conformation similar to that of diphosphorylated active ERK2 and the cAMP-dependent kinase catalytic subunit.²⁰ Thus, the diverse activation lip conformations in various inactive forms of MAPKs converge towards a uniform active state conformation that confers catalytic rate enhancement. This is expected because only a limited range of structures should produce catalytic function.²¹ In addition, active p38 γ MAPK shows greater closure between N- and C-terminal domains due to a rigid-body rotation of $>15^\circ$ compared to inactive p38 α MAPK, where the domains are held in an open conformation.²⁰ In contrast, structures of ERK2 show a smaller difference in domain rotation (5°) between active and inactive forms.⁴

To date, there is no information available as to whether phosphorylation-dependent changes in conformational mobility are also similar between different MAPKs. On one hand, MAPK family members share similarities in primary sequences, activation mechanisms, and structural motifs. On the other hand, small differences in sequence may yield large differences in the control of regional flexibility. Conceivably, the role that protein internal motions play in activation may differ significantly between these closely related enzymes.

Here, we investigate the effect of kinase activation on the conformational mobility of p38 α . By monitoring peptide sequences over the entire protein, we present a global picture of amide HX behavior and how this differs between active and inactive forms of the kinase. Overall, the patterns of in-exchange are similar between p38 α and ERK2, reflecting their similarities in sequence and structure. Upon p38 α activation, regional changes in HX are observed, some of which can be ascribed to changes in structure and others to conformational mobility. This suggests that kinase activation regulates mobility within localized regions. Importantly, the patterns of regulated mobility differ significantly between p38 α and ERK2. Thus, closely related MAPK family members show divergent behaviors with respect to the effects of phosphorylation and activation on protein motions.

Results

Achieving high coverage of exchangeable amide hydrogens

HX measurements were made by incubating protein in D₂O for varying periods of in-exchange. After quenching the in-exchange reaction, proteins were proteolyzed, and the extent of deuteration was quantified by liquid chromatography–mass spectrometry (LC-MS) measurements of peptides in the digest. High coverage of exchangeable amides over the protein sequence is needed in order to obtain a global view of amide HX behavior. In addition, because resolution is limited in peptides with large numbers of residues, greater recovery of peptides with overlapping sequences allows exchange behavior to be localized within narrower protein regions. Thus, techniques that maximize identification of peptides from proteolytic digests are needed to optimize HX measurements.

In an effort to maximize peptide identifications, we examined the influence of sampling, instrument, and peptide search algorithm on peptides observed in liquid chromatography–tandem mass spectrometry (LC-MS/MS) data sets of p38 α . Peptides present within protein digests are often missed because they fail to be identified with high confidence. Sampling

statistics often limit the number of peptides that are sequenced in any MS/MS run, when digests are complex. Low instrument sensitivity may limit the ability to sequence low-abundance ions. Finally, automated search programs may yield scores that are too low to confidently match peptide sequences to MS/MS spectra.

Three experiments were carried out to examine how each of these factors affects coverage and resolution (Fig. 1a). p38 α incubated in water was proteolyzed and peptides were sequenced by LC-MS/MS, identifying peptides using the Mascot search program. Two instrument platforms were used for LC-MS/MS. The QStar Pulsar is a quadrupole time-of-flight (TOF) mass spectrometer that is used to perform HX mass measurements by LC-MS, as well as LC-MS/MS sequencing. The LTQ-Orbitrap is an ion trap mass spectrometer that provides fast MS/MS scan rates, high sensitivity, and high mass accuracy. Peptides were then matched to those routinely observed in HX-MS data sets of p38 α incubated in D₂O to allow in-exchange. In each experiment, effects on sequence coverage and number of exchangeable amides were quantified.

The first experiment tested the effect of sampling on sequence coverage. Peptide identifications may be enhanced by repeating LC-MS/MS runs on the same digest, which increases sampling depth and the probability that an ion will be selected for MS/MS. LC-MS/MS performed on the Pulsar identified 39 peptides in a single run, yielding a 77% sequence coverage. Combining results from three or nine runs, respectively, yielded 77 peptides (88% sequence coverage) or 98 peptides (99% coverage) (Table 1, Supplementary Table 1). Of these, 30, 45, and 67 peptides, respectively, could be routinely identified in HX-MS data sets under conditions of p38 α deuteration. Therefore, increasing the depth of sampling by performing three or nine LC-MS/MS runs, respectively, improved peptide recovery by 1.5-fold or 2-fold over a single run, and increased the percentage of exchangeable amides observed from 64% to 81% or 95%. Not all peptides contributed to coverage; of the 30 peptides observed in a single LC-MS/MS run, 21 were sufficient to report 64% of exchangeable amides, while 9 peptides contained overlapping sequences that yielded no further sequence coverage but could be used to improve resolution. Of the 67 peptides observed in nine runs, 28 peptides covered 95% of exchangeable amides, while the rest contained overlapping sequences.

Peptide identifications may also be enhanced by fast scanning mass spectrometers that increase the number of MS/MS attempts in a single LC-MS/MS run. In a second experiment, we addressed the effects of instrument sensitivity and scan rate by analyzing p38 α digests on an LTQ-Orbitrap mass spectrometer, which is sensitive to low femtomoles and collects MS/MS ~4–5 times faster than the Pulsar. A single LC-MS/MS run identified 95 peptides, of which 61 were observable in HX-MS data sets, covering 72% of exchangeable amides (Table 1, Supplementary Table 1). Three LC-MS/MS runs yielded 110 peptides, of which 68 were observable in HX-MS data sets, representing 81% amide coverage. Thus, replicate runs on the LTQ-Orbitrap yielded greater numbers of peptides, consistent with the higher sensitivity and faster scan rate of this instrument. However, most of the additional peptides yielded overlapping sequence information, and, surprisingly, the amide coverage from peptides sequenced by the LTQOrbitrap was not significantly higher than that of the Pulsar. This suggested that another factor limits peptide identification.

A third experiment asked whether peptide identifications could be impacted using improved methods for matching MS/MS spectra to peptide sequences. Conventional search programs match m/z values between fragment ions observed in MS/MS spectra and those calculated from peptide sequences. This is the case for Mascot, which calculates MOWSE scores using a probabilistic model to evaluate the likelihood of observing fragments from a given sequence.²² Recent studies have shown that correct matches that fall below high-confidence MOWSE thresholds can be successfully captured using Similarity scores, which evaluate relative

intensities of fragment ions and m/z .^{23–25} We incorporated this principle into an in-house software named the Manual Analysis Emulator (MAE),²⁵ which uses the MassAnalyzer algorithm of Zhang to simulate relative intensities of fragment ions in theoretical MS/MS spectra and then rescores assignments made by Mascot using Similarity scoring.^{23,24} This has the effect of capturing peptides that are correct sequence assignments but are rejected because MOWSE scores are low.

The data sets from three LC-MS/MS runs on the LTQ-Orbitrap (Experiment 2) were rescored using MAE. By accepting assignments with either MOWSE or Similarity scores above high-confidence thresholds, 156 peptides were identified, covering 99% of the p38 α sequence (Table 1, Supplementary Table 1). Of these, 92 were observable in HX-MS data sets, representing 95% of exchangeable amides. Thus, improved scoring methods yielded higher data capture, so that the three LC-MS/MS runs on the LTQ-Orbitrap provided equivalent amide coverage and 60% more peptides with overlapping sequences, compared to nine LC-MS/MS runs on the Pulsar. As expected, the LTQ-Orbitrap experiments identified more ions with low intensity compared to the Pulsar experiments (data not shown), although very weak ions were often filtered out because they were not observed in HX-MS data sets. Importantly, our results suggest that MS/MS fragmentation differs between the LTQ and the Pulsar instruments in a way that differentially affects the resulting MOWSE scores. The fact that sequence coverages were similar between the LTQ-Orbitrap and the Pulsar in Experiments 1 and 2 implies that certain peptide sequences are less readily identified from MS/MS collected on the ion trap instrument, and that rescoring algorithms such as MAE are needed to capture these sequences.

Peptide yields are summarized in Fig. 1b and Supplementary Fig. 1, which show unique peptide sequences observed with each instrument, ignoring redundancies due to multiple ion forms with different charge states. A total of 175 peptides and 101 HX-MS-observable peptides were identified between the two instruments (Table 1). Of these, 45% of total peptides and 57% of HX-MS-observable peptides were observed by both instruments (Fig. 1b). Our combined data sets from 12 LC-MS/MS experiments yielded a 98% coverage of exchangeable amides (Table 1), with greater resolution due to overlapping peptides (Supplementary Fig. 1). High sequence coverage can be difficult to achieve in HX-MS studies, and coverage is often $\leq 50\%$, limiting the ability to survey events in the entire protein. Our analysis shows that sampling depth and search strategies are important factors to be considered in maximizing sequence coverage.

Amide HX in p38 α

p38 α was incubated in D₂O between 0 h and 4 h, and HX measurements were made on 101 peptides (Fig. 2). Deuteration at 4 h was then used to determine the extent of HX in localized regions of the protein, averaging the values for overlapping peptides. These were mapped against the backbone structure of p38 α (Fig. 3a).

Two regions of low HX (0–40%) were observed in p38 α . One was found in the C-terminal lobe and included the active-site $\beta 6$ strand and helices αE and αF , which form helix interactions with each other and connect to the active site. The second region included N-terminal strands $\beta 3$ and $\beta 4$, and intervening helix αC . In contrast, high levels of exchange were observed in regions with high solvent accessibility, including the activation lip, the MAPK insert, and various loops including the Gly-rich loop, which modulates ATP binding. Thus, the HX measurements revealed slow-exchanging core regions within both the N-terminal and the C-terminal domains of the bilobed structure and faster exchange within peripheral regions and loops. Regions within the active site containing the conserved catalytic base (Asp150-Leu-Lys) and Asp168-Phe-Gly motifs exchanged more slowly than the activation lip and the P + 1 substrate recognition site, with the latter undergoing almost complete exchange in 4 h. Overall, the pattern of regional HX was consistent with that expected from tertiary structure.

Comparison of HX in p38 α and ERK2

HX measurements of p38 α were compared to previous measurements of ERK2.⁷ The extents of protein deuteration at 4 h were similar, measured at 62% and 60% for p38 α and ERK2, respectively. In most regions, patterns of regional HX were similar between the two kinases. Thus, in both p38 α and ERK2, slower exchange was observed within the C-terminal core encompassing the catalytic site, α E, and α F, as well as the N-terminal core containing β 3– α C– β 4, while faster exchange occurred within peripheral regions and loops, as well as within the MAPK insert (Fig. 3a and b).

Two exceptions were helix α D and C-terminal helix α L16, where, in each case, the percentage deuterations in p38 α and ERK2 differed by >40%. In helix α D, 84% of exchangeable amides were deuterated after 4 h in p38 α , in contrast to 39% in ERK2. This correlated well with regional differences in main-chain *B*-factors within helix α D, which were higher in p38 α (37–76 Å²) than in ERK2 (15–38 Å²) (Fig. 3c and d). Calculation of the distance of each amide to the solvent-accessible surface (distance-to-surface), as well as the length and orientation of amide hydrogen bonds, showed similar structures and solvent accessibility of amide hydrogens within helix α D between the two kinases. This suggests that side-chain interactions in p38 α confer greater mobility within α D, whereas the same region is less dynamic in ERK2.

Helix α L16 represents the C-terminal extension in MAPKs, interacting with the N-terminal lobe in a pocket formed between the β 3– β 4– β 5 sheet and helix α C. In p38 α , helix α L16 exchanges slowly, with 10% deuteration after 4 h, whereas in ERK2, >58% of amides in the same region undergo deuteration. This difference was not reflected by *B*-factors (Fig. 3c and d), nor was it predicted from structure, where distance-to-surface and hydrogen bonding of amide hydrogens within α L16 showed very similar patterns between the two kinases. We infer that the conformational mobility of α L16 in solution is significantly lower in p38 α than in ERK2.

Taken together, the HX measurements reveal that regional conformational mobility is conserved between p38 α and ERK2 MAPKs, reflecting conservation of sequence and tertiary structure. Differences were noted in helix α D, where p38 α showed higher mobility compared to ERK2—an effect recapitulated in *B*-factor measurements. It was noteworthy that *B*-factors also predicted the high degree of HX observed within the activation lip of p38 α , as well as the Gly-rich loop and other β -sheet loops within the N-termini of both enzymes. However, *B*-factors in α L16 were unable to predict differences in conformational mobility between p38 α and ERK2, and were also inconsistent with high levels of HX observed within the activation lip and the P + 1 loop of ERK2, or the MAPK insert in either enzyme. Overall, whereas the patterns of HX showed strong similarities between p38 α and ERK2, the *B*-factor patterns appeared more divergent.

Regional HX is altered by phosphorylation and activation of p38 α

HX measurements were compared between unphosphorylated (0P) and diphosphorylated (2P) forms of p38 α , in order to define regions responsive to kinase activation. Sites of proteolytic cleavage were nearly identical between the two forms. The sole exception was the activation lip, where several cleavage sites surrounding the Thr-Xxx-Tyr region in 0P-p38 α were masked from proteolysis in 2P-p38 α (Fig. 2). This may be explained by altered proteolytic specificity by phosphorylation, or conformational changes that convert a proteolytically accessible activation lip in 0P-p38 α into a more protected conformation in 2P-p38 α .

Of the 101 peptides, 32 showed significant differences in deuteration between active *versus* inactive p38 α , where, in all cases, HX decreased upon enzyme activation (Fig. 2, green). Many

of these peptides overlapped in sequence; in all, 10 peptides were sufficient to summarize the changes in HX (Fig. 4).

Differences in HX either reflect changes in conformation upon p38 α activation or, alternatively, report changes in conformational mobility and internal motions of the folded state. In order to evaluate contributions from structural changes, X-ray coordinates of unphosphorylated p38 α (1P38; Wang *et al.*¹⁵) were compared to those of diphosphorylated p38 γ (1CM8; Bellon *et al.*²⁰) in regions where HX decreased upon p38 α activation. The lip and catalytic site structures in p38 γ overlay well with those in diphosphorylated ERK2 and cAPK,²⁰ providing a reasonable prediction of how p38 α would undergo conformational remodeling upon phosphorylation. Outside the lip and catalytic site, backbone conformations of active p38 γ and inactive p38 α resemble each other closely, with rmsd of 1.2 Å and 0.62 Å when N- and C-terminal domains are, respectively, superimposed between each enzyme.²⁰ Thus, the difference in domain angle between these kinases reflects rigid-body movements of the N- and C-terminal lobes.

Peptides displaying the greatest changes in HX were located within five regions (Figs. 5–9):

1. Activation lip and P+1 specificity site: Peptide residues (pr) 165–187 (KILDFGLARHTDDEMTGYVATRW) contain the activation lip, with residues comprising the conserved Asp-Phe-Gly motif and Thr-Xxx-Tyr phosphorylation sites. Here, the pepsin cleavage sites differed between 0P-p38 α and 2P-p38 α (Fig. 2). Therefore, we compared the deuteration time course of pr165–187 observed as a single intact peptide in 2P-p38 α to a corresponding time course calculated by summing the deuteration of two peptides in 0P-p38 α (Fig. 5a). The time course of pr165–182+pr183–187 in 0P-p38 α showed higher deuteration than that of pr165–187 from 2P-p38 α , despite the fact that the time course represented by composite sequences contained one less exchangeable amide. This confirms that HX decreases significantly within the activation lip in 2P-p38 α . Adjacent to this region is pr188–195 (YRAPEIML), which forms the P+1 substrate recognition site. Direct comparison of the same peptide between 0P-p38 α and 2P-p38 α revealed significantly decreased HX in active p38 α (Fig. 5b). The X-ray structures of p38 α and phosphorylated p38 γ predict substantial conformational remodeling of this region upon kinase phosphorylation (Fig. 5c). In the 0P-p38 α structure, residues 171–179 are highly exposed to solvent with large main-chain *B*-factors (80 Å²), whereas in 2P-p38 γ , the activation lip is more constrained with lower *B*-factors (45–70 Å²). Residues within pr188–195, which are accessible to solvent in 0P-p38 α , are buried in 2P-p38 γ due to movement of the activation lip. Such changes in conformation readily account for the significant decrease in HX observed in this region upon p38 α activation. Domain closure between N- and C-terminal lobes observed in 2P-p38 γ may also reduce the solvent accessibility of residues in the lip.²⁰ Thus, the effect of p38 α phosphorylation on HX occurring within the lip and the P+1 loop can be attributed to structural remodeling of the activation lip, as well as interdomain interactions that accompany dual phosphorylation.
2. C-terminal helix α E and catalytic site β 6: Decreased HX was observed in pr130–145 (LIYQILRGLKYIHSAD), which includes most of helix α E, and pr146–156 (IIHRDLKPSNL), which contains the β 6-strand and the catalytic base Asp150 (Fig. 6a and b). Helix α E forms core α -helix interactions that stabilize the C-terminal domain, and residues in helix α E are deeply buried in p38 α , with amide hydrogens typically removed from the surface by 4–7 Å. 2P-p38 γ shows no obvious changes in distance-to-surface or hydrogen bonding patterns in this region (Fig. 6c). Thus, the significant decrease in HX upon phosphorylation suggests lower conformational mobility in active p38 α , enhancing stability of the C-terminal core. Strand β 6 forms interactions with the activation lip upon p38 α phosphorylation, through ion pair

interactions between Arg149 and lip residue pThr180, which may constrain mobility within $\beta 6$ (Fig. 6c). Side-chain interactions between helix αE and strand $\beta 6$ (Fig. 6d) suggest connections between these regions that may explain their correlated decreases in HX.

3. C-terminal extension and the L16 loop: pr327–333 (FESRDLL) in the p38 α structure contains a single 3–10 helical turn at the end of the C-terminal extension, terminating in helix $\alpha L16$, where HX decreases upon kinase activation (Fig. 7a). This region is disordered in 2P-p38 γ ; thus, structural comparisons cannot be made. Nevertheless, much is known about this region, which has been implicated in p38 α activation via a cluster of hydrophobic residues involving interactions between Phe327 located within this region and Tyr323 located upstream, Trp337 in helix $\alpha L16$, and Tyr69 in helix αC (Fig. 7b).^{26–28} Diskin *et al.* have shown that mutating Phe327 to Leu or Ser causes p38 α autoactivation by promoting autophosphorylation at Thr180, and X-ray evidence shows that these mutations disrupt residue interactions within the hydrophobic cluster (Fig. 7c; Diskin *et al.*).^{26,27} This in turn disrupts ion pair interactions of the adjacent residue Glu328 with Arg70 in helix αC , which, in 0P-p38 α , are separated by 2.9 Å. We speculate that release of Arg70 would enable rotation of helix αC , allowing formation of ion pair interactions with pThr180, as seen in the Arg70-pThr180 distance of 2.9 Å in 2P-p38 γ (Fig. 7c). This model suggests that the hydrophobic cluster constrains interactions between helix αC and the activation lip by sequestering Arg70. Therefore, it is reasonable to expect that phosphorylation of Thr180 at the activation lip would favor Arg70-pThr180 interactions, disrupting interactions between the hydrophobic cluster residues and promoting interdomain closure. We hypothesize that the observed decrease in HX in the 3–10 helix reflects conformational changes induced by remodeling of the hydrophobic cluster. The 3–10 helix in p38 α resembles an analogous turn in the X-ray structure of phosphorylated ERK2.⁴ In ERK2, the 3–10 turn is found uniquely in the phosphorylated kinase and forms a surface for dimerization, where hydrophobic side chains in this region interdigitate with corresponding residues from a second subunit. It has, in fact, been suggested that activating mutations facilitate p38 α dimerization, given that autoactivation involves transphosphorylation between kinase subunits,²⁶ although no evidence for dimerization was apparent in the X-ray structure of 2P-p38 γ or by size exclusion chromatography of 2P-p38 α .^{20,29} We therefore examined the possibility that p38 α dimerizes following phosphorylation, and that the decrease in HX in pr327–333 might report steric protection from solvent in the dimer. Unphosphorylated and diphosphorylated forms of p38 α were examined by sedimentation equilibrium (Fig. 7d and e). Both forms of p38 α were monomeric under all conditions. Thus, wild-type p38 α does not dimerize upon phosphorylation, and the decrease in HX in this region can instead be attributed to conformational changes in monomer.
4. N-terminal $\beta 4$ – $\beta 5$ strands and helices $\alpha L16$ and αC : pr88–103 (DVFTPARSLEEFNDVY) contains strands $\beta 4$ – $\beta 5$ and the intervening loop, which is largely exposed to solvent. Kinase activation leads to decreased HX in this region (Fig. 8a). Decreased HX is also observed in pr344–348 (EVISF) (Fig. 8b), which represents the C-terminal helix $\alpha L16$, a structural motif common to MAPK family members. pr72–86 (LRLKHKHENVIGL), containing the αC – $\beta 4$ loop, shows decreased HX, whereas overlapping pr75–86 does not (Fig. 8c and d), indicating that the decreased HX can be narrowed to amide residues 72–75 within helix αC (LRL). These regions form side-chain interactions with each other within the N-terminal lobe, involving connections between Leu72 in helix αC ; Val89, Leu96, and Phe99 in $\beta 4$ – $\beta 5$; and Tyr342, Val345, Ile346, and Phe348 within $\alpha L16$ (Fig. 8e). Therefore, correlated decreases in HX in both regions may reflect coupling between these regions through hydrophobic side-chain interactions. C $^{\alpha}$ structures within this region show a

high overlap between 0P-p38 α and 2P-p38 γ (Fig. 8f), suggesting that decreased HX may be accounted for by flexibility changes following phosphorylation, although perturbations in this region might also result from helix α C movements accompanying domain closure.

5. Substrate-binding sites: strands β 7– β 8 and helices α F– α G: pr217–234 (LTGRTLFPGTDHIDQLKL) contains part of conserved helices α F and α G and the intervening loop, and forms an extended surface for interactions with the activation lip of the p38 α substrate, MAPKAP kinase 2 (MK2).^{18,19} pr157–164 (AVNEDCEL) forms part of the binding site for a docking motif (“DEJL” motif) composed of a cluster of basic residues, followed by the L/I-X-L/I sequence found in substrates and regulatory proteins such as scaffold and adaptor proteins, MAPK kinases, and MAPK phosphatases.^{30,31} Both the α F– α G loop and the DEJL-binding site form major contacts for binding p38 α to MK2.^{18,19} The interactions stabilize a high-affinity inactive p38 α –MK2 complex localized to the nucleus, which, upon phosphorylation of p38 α , becomes disrupted, enabling phosphorylation and nuclear export of MK2.^{18,32} The α F– α G loop residue Thr218 also forms a partial interaction surface for the allosteric effector TAB1, which selectively binds p38 α through a modified docking interaction extending from this region to the nearby DEJL motif-binding site.^{33,34} In both regions, HX decreased upon p38 α phosphorylation (Fig. 9a and b). Inspection of 0P-p38 α and 2P-p38 γ showed little differences in structure within the α F– α G and β 7– β 8 loop regions (Fig. 9c and d). However, in 0P-p38 α , the activation lip residue Tyr182 makes close contacts with α F– α G loop residues Gly225–Thr226, burying the amide hydrogen at residue Thr226 (Fig. 9c). Remodeling of the activation lip in 2P-p38 γ disrupts this interaction, exposing the amide to solvent. Interestingly, HX decreased significantly in 2P-p38 α , despite the predicted increase in solvent accessibility in this region upon kinase phosphorylation. The lack of concurrence between HX behavior and expected structural changes suggests that protein mobility in these regions decreases upon p38 α activation, although structural differences between 2P-p38 γ and 2P-p38 α cannot be ruled out. Conceivably, decreased flexibility within these binding sites might affect the binding of substrate or TAB1 by reducing their interactions with the active form of p38 α .

HX in monophosphorylated p38 α

Phosphorylation of p38 α occurs preferentially at Tyr182, and p38 α -pTyr182 is the predominant monophosphorylated form in stress-treated cells and *in vitro* reactions with MKK3/6.^{29,35} Therefore, we examined HX behavior on p38 α monophosphorylated at Tyr182 (0.85 mol/mol). Figure 10 shows results for seven peptides, where the largest change in HX was observed in active p38 α , decreasing deuteration either by >50% or by >2 Da over the time course. In each case, time courses of deuteration in monophosphorylated p38 α resembled those in unphosphorylated p38 α more than diphosphorylated enzyme. This occurred in the activation lip and the P+1 site, as well as in the substrate-binding sites, the N- and C-terminal core regions, and the C-terminal 3–10 helix. This indicates that the conformational and dynamic responses underlying the changes in HX result from phosphorylation at both Thr180 and Tyr182.

Discussion

HX measurements reveal information about the conformational mobility of proteins in solution and are complementary to structural analysis of low-energy conformers by X-ray crystallography. Analysis of p38 α reveals slow-exchanging core regions composed of β 6, α E, and α F in the C-terminal domain, and β 3, β 4 and α C in the N-terminal domain. In contrast, greater levels of exchange were observed in the activation lip, the MAPK insert, and peripheral loops where the structure would predict higher solvent accessibility. Thus, an important finding

from this study is that patterns of regional HX in p38 α are consistent with tertiary structure. With only a few exceptions, the HX patterns in p38 α closely resemble those in ERK2, demonstrating that regional conformational mobility is conserved between these two MAPKs, as one might expect based on their conserved sequences and tertiary structures.

A key finding is that HX rates are altered in response to phosphorylation, reflecting changes in structure and conformational mobility upon kinase activation. These can be interpreted by comparing X-ray structures of 0P-p38 α and 2P-p38 γ , and by incorporating information from prior enzymatic studies. Altered HX within the activation lip, the P+1 loop, and the active site (β 6) is consistent with expected conformational remodeling of the activation lip following phosphorylation. Likewise, changes in HX within the 3–10 helix most likely reflect conformational changes within an N-terminal hydrophobic cluster described by Diskin *et al.*, which might undergo residue displacement upon activation lip phosphorylation.^{26,27} In contrast, other regions show changes in HX that cannot be readily explained by structural rearrangements, and may instead reflect changes in protein internal motions or flexibility responsive to phosphorylation. These are found in binding sites for substrates and allosteric regulators, N-terminal regions that link the core β 4– β 5 strand to helices α L16 and α C, and the C-terminal core helix α E. Modulation of protein motions in these regions could contribute to kinase regulation, where decreased protein flexibility in localized regions might somehow facilitate substrate binding and turnover.

HX behavior of 1P-p38 α suggests a mechanism paralleling models of lip reorganization in ERK2. X-ray structures of unphosphorylated and diphosphorylated ERK2 show stable activation lip structures,^{3,4} and enzymatic measurements show that phosphorylation at Tyr185 is kinetically preferred.³⁶ In contrast, in X-ray structures of ERK2 mutants replacing the Thr-Glu-Tyr sequence at the activation lip with acidic residues, the activation lip becomes highly disordered.³⁷ Main-chain *B*-factors increase by $>35 \text{ \AA}^2$ and 55 \AA^2 in the structures of ERK2-Tyr185Glu and Thr183Glu/Tyr185Glu, respectively. The results suggest that ERK2 undergoes phosphorylation at one residue (preferentially at Tyr), which increases mobility within the activation lip. The lip then remodels into a stable active configuration following phosphorylation at the second residue. Thus, both phosphorylation events are needed for the dramatic change in lip conformation during kinase activation. In p38 α , the activation lip is already disordered and highly exposed to solvent in the unphosphorylated form.^{15,16} By analogy with ERK2, incorporation of one phosphate would produce little change in lip stability, until incorporation of the second phosphate tethers the lip into an active conformation. This would explain why HX of monophosphorylated p38 α more closely resembles that of the unphosphorylated enzyme. Our data suggest that HX in p38 α is mainly regulated by conformational changes following dual phosphorylation, which anchor the lip into the active conformation.

Importantly, patterns of HX regulated by activation show significant differences between p38 α and ERK2. As expected, both enzymes show perturbations within the activation lip, corresponding to lip remodeling. In addition, both enzymes share patterns of decreased HX in the α F– α G loop region. Regulated motions in this region may be important to modulating interactions between MAPK substrates and allosteric regulators such as TAB1. However, in contrast to p38 α , ERK2 activation leads to increased HX within the hinge, the Gly-rich loop, and the MAPK insert (Fig. 11). Differences in HX regulation in corresponding regions of p38 α may reflect differences between these enzymes in mechanisms underlying enzyme activation. For example, the ERK2 hinge represents a region of regulated flexibility that can be linked to interdomain interactions responsive to activity state.¹⁴ X-ray structures of inactive p38 α show a wider domain separation than ERK2, as well as hinge rotation allowing hinge residues to interfere with adenine ring interactions.^{15,16} Thus, p38 α retains an open conformation, even when bound to ATP-competitive inhibitors or upon MK2 substrate binding.

^{18,19,38} Such constraints prevent domain closure and probably preclude regulation of HX upon activation lip phosphorylation. As a result, ATP binding affinity increases substantially upon activation of p38 α (also seen in p38 γ), whereas ERK2 shows little change in ATP binding upon activation.^{3,14,39,40}

The ability to monitor protein flexibility and mobility by HX adds a new dimension towards understanding how kinases are controlled. The regulated motions revealed by HX alterations upon kinase activation are dissimilar between ERK2 and p38 α , which are closely related in sequence, tertiary structure, and dual-phosphorylation mechanism. We conclude that while patterns of solvent accessibility may be conserved between related enzymes, patterns of activation-induced motional changes are not conserved. Our findings provide evidence that MAPKs diverge with respect to regulation of internal protein motions and their potential contribution to function.

Materials and Methods

Proteins

Doubly phosphorylated active kinase (2P-p38 α) was produced in BL21(DE3)-pLysS using the plasmid pET (His)-MKK6DD/p38 α , which expresses wild-type mouse His6-p38 α and constitutively active MKK6, as previously described.⁴¹ Unphosphorylated inactive kinase (0P-p38 α) was produced in pET(His)-MKK6DD/p38 α , modified by deleting the MKK6 open reading frame. Monophosphorylated inactive kinase (1P-p38 α) was produced in pET(His)-MKK6DD/p38 α , modified by inserting a stop codon at residue Tyr64 of MKK6. Each kinase was purified using Ni-NTA agarose (Qiagen) chromatography and MonoQ FPLC;¹⁴ dialyzed overnight in 50 mM KPO₄ (pH 7.4), 100 mM KCl, and 5 mM dithiothreitol; and stored in aliquots at -80 °C. MS confirmed phosphorylation stoichiometry at the activation lip, where 0P-p38 α was >99% unphosphorylated, 2P-p38 α was >99% diphosphorylated at Thr180 and Tyr182, and 1P-p38 α was 85% monophosphorylated at Tyr182 and 5.5% monophosphorylated at Thr180 (data not shown).

HX-MS measurements

Data collection and analysis of weighted average mass, in-exchange, and back-exchange were performed as described.⁴²⁻⁴⁴ Data were collected on a QStar Pulsar QqTOF MS interfaced with an Agilent Cap1100 HPLC (500 μ m i.d. \times 10 cm column, packed with POROS R1 20 resin). Proteins (4 μ g) were incubated in 90% D₂O at 10 °C, allowing the in-exchange reaction to take place from 8 s to 4 h. Reactions were quenched with 90 μ l of 25 mM succinic acid and 25 mM citric acid (pH 2.4), and cooled rapidly to 0 °C. Proteins were digested by adding 10 μ l of pepsin (4 μ g) and were analyzed by LC-MS. Time-zero measurements were performed by quenching the reaction before adding D₂O. Samples were randomized to control for systematic variations, and replicate runs were performed at 0 s, 60 s, and 1800 s. Across all time points, the average standard deviation of weighted average mass was 0.05 Da, with a maximum standard deviation of 0.13 Da (Supplementary Table 3). Deuteration time courses were corrected for artifactual in-exchange and back-exchange, then fitted to a sum of exponentials.

Weighted average mass calculations were carried out using HX-Analyzer, an interactive tool for increasing the accuracy and speed of analysis of HX-MS data, developed in-house and implemented in Visual Basic using ABI Analyzer QS, MS Office XP, and MS XP software library modules. HX-Analyzer inputs a list of LC-MS/MS files (.wiff) and a spreadsheet summarizing information about peptide ion mass and approximate elution time, presents isotopic peaks for examination across several data sets for manual inspection, and then outputs isotopic masses and weighted average mass for each peptide ion. HX time courses were fitted

by nonlinear least squares to the equation $Y = N - Ae^{-k_1t} - Be^{-k_2t} - Ce^{-k_3t}$, where Y is the number of deuterons exchanged at time t ; A , B , and C are the numbers of backbone amides exchanging at rates k_1 , k_2 , and k_3 , respectively; and N is the maximal deuteration over the experimental time period ($N = A + B + C$). Subtracting N from the total number of exchangeable backbone amides yields NE, the number of amides that are nonexchanging over the experimental time period.^{43,44} Nonlinear least squares curve fitting was performed, and results were plotted using Sigmaplot (SPSS Inc.). Fitted kinetic parameters are shown in Supplementary Table 2.

For LC-MS/MS, proteins incubated in water were treated and proteolyzed as described above. Samples (4 μ g) were analyzed on the Pulsar mass spectrometer with an m/z window of 400–1600 Da, a duty cycle of 15.5 s, and three MS/MS per cycle. Samples (60 ng) were analyzed on the LTQ-Orbitrap mass spectrometer interfaced with an Eksigent 2DLC HPLC (75 μ m i.d. \times 150 mm column, Zorbax C18 resin), with an m/z window of 300–2000 Da, a duty cycle of 4–6 s (\sim 10–14 cycles/min), and five MS/MS per cycle. MS/MS were converted to .mgf files and searched against the p38 α sequence using the Mascot search program (v. 1.9), with no enzyme specified. Mass tolerances used for Pulsar data sets were 2.5 Da for parent ions and 1.2 Da for fragment ions. Mass tolerances for LTQ-Orbitrap data sets were 1.2 Da for parent ions and 0.8 Da for fragment ions. The MAE was used to generate theoretical spectra for the top two sequence assignments made by Mascot, and Similarity scores evaluating overlap between theoretical and observed spectra were calculated as described.²⁵ The high-confidence thresholds used were MOWSE = 30 and Similarity = 0.5, which yielded a false discovery rate of 0.3%.

Analytical ultracentrifugation equilibrium experiments

Sedimentation equilibrium analyses were performed on a Beckman Proteomelab XLI analytical ultracentrifuge with absorbance optics at 280 nm for the detection of aromatic residues. Samples were loaded into 12-mm Epon cells at concentrations ranging from 0.32 mg/ml to 0.44 mg/ml. The samples were then centrifuged at 20 °C at 20,000g, 24,000g, and 28,000g for 24 h to achieve equilibrium, and successive radial absorbance scans were recorded. Protein molecular weights and oligomerization behavior were determined by fitting the sedimentation equilibrium data from different initial loading concentrations and rotor speeds to various monomer–oligomer equilibrium schemes using WIN NonLIN (v. 1.035, University of Connecticut) fitted to theoretical partial specific volumes based on compositions.⁴⁵ The partial specific volume of the sample and the density of the buffer were calculated using SednTerp (v. 1.06, University of New Hampshire) using the weighted average of the amino acid content. To obtain the observed molecular weight, dissociation constants, oligomerization states, and absorbance results were converted to linear plots of $\ln(AU)$ versus r^2 (radius) to the theoretical monomer and dimer (single-species models) using the equation:

$$C_r = C_0 \exp \left[M \left((1 - v_{\text{bar}}) \rho \right) \omega^2 \left(r^2 - r_0^2 \right) / 2RT \right]$$

where C_r is the concentration at radius $r(A)$, C_0 is the concentration at the meniscus, M is the monomer molecular weight, v_{bar} is the partial specific volume calculated by SednTerp, ρ is the buffer density, and ω is the angular velocity.

Supplementary Material

Refer to Web version on PubMed Central for supplementary material.

Acknowledgments

We are indebted to Stephane Houel for LTQ-Orbitrap data collection, and to Brian Eichelberger and William Old for help with data analysis. We also thank Melanie Cobb and Elizabeth Goldsmith (University of Texas Southwestern) for generously providing pET(His)-p38 α and pET(His)-MKK6DD/p38 α plasmids. This work was supported by National Institutes of Health awards R01 GM074134 (N.G.A.) and R01 CA126240 (K.A.R.).

Abbreviations used

MAPK, MAP kinase
HX, hydrogen exchange
ERK, extracellular-signal-regulated kinase
JNK, Jun N-terminal kinase
HX-MS, hydrogen-exchange mass spectrometry
LC-MS, liquid chromatography–mass spectrometry
LC-MS/MS, liquid chromatography–tandem mass spectrometry
TOF, time of flight
MAE, Manual Analysis Emulator
pr, peptide residue
MK2, MAPKAP kinase 2

References

1. Lee JC, Kumar S, Griswold DE, Underwood DC, Votta BJ, Adams JL. Inhibition of p38 MAP kinase as a therapeutic strategy. *Immunopharmacology* 2000;47:185–201. [PubMed: 10878289]
2. Johnson DA, Akamine P, Radzio-Andzelm E, Madhusudan M, Taylor SS. Dynamics of cAMP-dependent protein kinase. *Chem. Rev* 2001;101:2243–2270. [PubMed: 11749372]
3. Zhang F, Strand A, Robbins D, Cobb MH, Goldsmith EJ. Atomic structure of the MAP kinase ERK2 at 2.3 Å resolution. *Nature* 1994;367:704–711. [PubMed: 8107865]
4. Canagarajah BJ, Khokhlatchev A, Cobb MH, Goldsmith EJ. Activation mechanism of the MAP kinase ERK2 by dual phosphorylation. *Cell* 1997;90:859–869. [PubMed: 9298898]
5. Lee T, Hoofnagle AH, Kabuyama Y, Stroud J, Min X, Goldsmith EJ, et al. Docking motif interactions in MAP kinases revealed by hydrogen exchange mass spectrometry. *Mol. Cell* 2004;14:43–55. [PubMed: 15068802]
6. Resing K, Ahn NG. Deuterium exchange mass spectrometry as a probe of protein kinase activation. Analysis of wild-type and constitutively active mutants of MAP kinase kinase-1. *Biochemistry* 1998;37:463–475. [PubMed: 9425067]
7. Hoofnagle AN, Resing KA, Ahn NG. Changes in protein conformational mobility upon activation of extracellular regulated protein kinase-2 as detected by hydrogen exchange. *Proc. Natl. Acad. Sci. U. S. A* 2001;98:956–961. [PubMed: 11158577]
8. Hoofnagle AH, Resing KA, Ahn NG. Protein analysis by hydrogen exchange mass spectrometry. *Annu. Rev. Biophys. Biomol. Struct* 2003;32:1–25. [PubMed: 12598366]
9. Busenlehner LS, Armstrong RN. Insights into enzyme structure and dynamics elucidated by amide H/D exchange mass spectrometry. *Arch. Biochem. Biophys* 2005;433:34–46. [PubMed: 15581564]
10. Hamuro Y, Zawadzki KM, Kim JS, Stranz DD, Taylor SS, Woods VL. Dynamics of cAPK type II β activation revealed by enhanced amide H/2H exchange mass spectrometry (DXMS). *J. Mol. Biol* 2003;327:1065–1076. [PubMed: 12662931]
11. Wong L, Lieser S, Chie-Leon B, Miyashita O, Aubol B, Shaffer J, et al. Dynamic coupling between the SH2 domain and active site of the COOH terminal Src kinase, Csk. *J. Mol. Biol* 2004;341:93–106. [PubMed: 15312765]
12. Alverdi V, Mazon H, Versluis C, Hemrika W, Esposito G, van den Heuvel R, et al. cGMP binding prepares PKG for substrate binding by disclosing the C-terminal domain. *J. Mol. Biol* 2007;375:1380–1393. [PubMed: 18082764]

13. Hoofnagle AH, Stoner JW, Lee T, Eaton SS, Ahn NG. Phosphorylation-dependent changes in structure and dynamics in ERK2 detected by SDSL and EPR. *Biophys. J* 2004;86:395–403. [PubMed: 14695281]
14. Lee T, Hoofnagle AN, Resing KA, Ahn NG. Hydrogen exchange solvent protection by an ATP analogue reveals conformation change in ERK2 upon activation. *J. Mol. Biol* 2005;353:600–612. [PubMed: 16185715]
15. Wang Z, Harkins PC, Ulevitch RJ, Han J, Cobb MH, Goldsmith EJ. The structure of mitogen-activated protein kinase p38 at 2.1Å resolution. *Proc. Natl. Acad. Sci. U. S. A* 1997;94:2327–2332. [PubMed: 9122194]
16. Wilson KP, Fitzgibbon MJ, Caron PR, Griffith JP, Chen W, McCaffrey PG, et al. Crystal structure of p38 mitogen-activated protein kinase. *J. Biol. Chem* 1996;271:27696–27700. [PubMed: 8910361]
17. Xie X, Gu Y, Fox T, Coll JT, Fleming MA, Markland W, et al. Crystal structure of JNK3: a kinase implicated in neuronal apoptosis. *Structure* 1998;6:983–991. [PubMed: 9739089]
18. ter Haar E, Prabhakar P, Liu X, Lepre C. Crystal structure of the p38 alpha-MAPKAP kinase 2 heterodimer. *J. Biol. Chem* 2007;282:9733–9739. [PubMed: 17255097]
19. White A, Pargellis CA, Studts JM, Werneburg BG, Farmer BT. Molecular basis of MAPK-activated protein kinase 2: p38 assembly. *Proc. Natl. Acad. Sci. U. S. A* 2007;104:6353–6358. [PubMed: 17395714]
20. Bellon S, Fitzgibbon MJ, Fox T, Hsiao HM, Wilson KP. The structure of phosphorylated p38 gamma is monomeric and reveals a conserved activation-loop conformation. *Structure* 1999;7:1057–1065. [PubMed: 10508788]
21. Nolen B, Taylor S, Ghosh G. Regulation of protein kinases; controlling activity through activation segment conformation. *Mol. Cell* 2004;15:661–675. [PubMed: 15350212]
22. Perkins DN, Pappin JC, Creasy DM, Cottrell JS. Probability-based protein identification by searching sequence databases using mass spectrometry data. *Electrophoresis* 1999;20:3551–3567. [PubMed: 10612281]
23. Zhang Z. Prediction of low-energy collision-induced dissociation spectra of peptides. *Anal. Chem* 2004;76:3908–3922. [PubMed: 15253624]
24. Zhang Z. Prediction of low-energy collision-induced dissociation spectra of peptides with three or more charges. *Anal. Chem* 2005;77:6364–6373. [PubMed: 16194101]
25. Sun S, Meyer-Arendt K, Eichelberger B, Brown B, Yen CY, Old W, et al. Improved validation of peptides MS/MS assignments using spectral intensity prediction. *Mol. Cell. Proteomics* 2006;6:1–17. [PubMed: 17018520]
26. Diskin R, Lebendiker M, Engelberg D, Livnah O. Structures of p38alpha active mutants reveal conformational changes in the L16 loop that induce autophosphorylation and activation. *J. Mol. Biol* 2007;365:66–76. [PubMed: 17059827]
27. Diskin R, Askari N, Capone R, Engelberg D, Livnah O. Active mutants of the human p38a mitogen-activated protein kinase. *J. Biol. Chem* 2004;279:47040–47049. [PubMed: 15284239]
28. Avitzour M, Diskin R, Raboy B, Askari N, Engelberg D, Livnah O. Intrinsically active variants of all human p38 isoforms. *FEBS J* 2007;274:963–975. [PubMed: 17241234]
29. Doza YN, Cuenda A, Thomas GM, Cohen P, Nebreda AR. Activation of the MAP kinase homologue RK requires the phosphorylation of Thr-180 and Tyr-182 and both residues are phosphorylated in chemically stresses KB cells. *FEBS Lett* 1995;364:223–228. [PubMed: 7750576]
30. Tanoue T, Adachi M, Moriguchi T, Nishida R. A conserved docking motif in MAP kinases common to substrates, activators and regulators. *Nat. Cell Biol* 2000;2:110–116. [PubMed: 10655591]
31. Chang CI, Xu BE, Akella R, Cobb MH, Goldsmith EJ. Crystal structure of MAP kinase p38 complexed to the docking sites on its nuclear substrate MEF2A and activator MKK3B. *Mol. Cell* 2002;9:1241–1249. [PubMed: 12086621]
32. Engel K, Kotlyarov A, Gaestel M. Leptomycin B-sensitive nuclear export of MAPKAP kinase 2 is regulated by phosphorylation. *EMBO J* 1998;17:3363–3371. [PubMed: 9628873]
33. Ge B, Gram H, DiPadova F, Huang B, New L, Ulevitch RJ, et al. MAPKK-independent activation of p38alpha mediated by TAB1-dependent autophosphorylation of p38alpha. *Science* 2002;295:1291–1294. [PubMed: 11847341]

34. Zhou H, Zheng M, Chen J, Changchuan X, Kolatkar AR, Zarubin T, et al. Determinants that control the specific interactions between TAB1 and p38 α . *Mol. Cell. Biol* 2006;26:3824–3834. [PubMed: 16648477]
35. Raingeaud J, Gupta S, Rogers JS, Dickens M, Han J, Ulevitch RJ, Davis RJ. Pro-inflammatory cytokines and environmental stress cause p38 mitogen activated protein kinase activation by dual phosphorylation on tyrosine and threonine. *J. Biol. Chem* 1995;270:7420–7426. [PubMed: 7535770]
36. Haystead TA, Dent P, Wu J, Haystead CM, Sturgill TW. Ordered phosphorylation of p42mapk by MAP kinase kinase. *FEBS Lett* 1992;306:17–22. [PubMed: 1628739]
37. Zhang J, Zhang F, Ebert D, Cobb MH, Goldsmith EJ. Activity of the MAP kinase ERK2 is controlled by a flexible surface loop. *Structure* 1995;3:299–307. [PubMed: 7540485]
38. Wang Z, Canagarajah BJ, Boehm JC, Kassisà S, Cobb MH, Young PR, et al. Structural basis of inhibitor selectivity in MAP kinases. *Structure* 1998;6:1117–1128. [PubMed: 9753691]
39. Frantz B, Klatt T, Pang M, Parsons J, Rolando A, Williams H, et al. The activation state of p38 mitogen-activated protein kinase determines the efficiency of ATP competition for pyridinylimidazole inhibitor binding. *Biochemistry* 1998;37:13846–13853. [PubMed: 9753474]
40. Fox T, Fitzgibbon MJ, Fleming MA, Hsiao HM, Brummel CL, Su MSS. Kinetic mechanism and ATP binding site reactivity of p38 γ MAP kinase. *FEBS Lett* 1999;461:323–328. [PubMed: 10567720]
41. Wilsbacher JL, Cobb MH. Bacterial expression of activated mitogen-activated protein kinases. *Methods Enzymol* 2001;332:387–400. [PubMed: 11305113]
42. Resing KA, Hoofnagle AN, Ahn NG. Modeling deuterium exchange behavior of ERK2 using pepsin mapping to probe secondary structure. *J. Am. Soc. Mass Spectrom* 1999;10:685–702. [PubMed: 10439507]
43. Hoofnagle AN, Resing KA, Ahn NG. Practical methods for deuterium exchange/mass spectrometry. *Methods Mol. Biol* 2003;250:283–298. [PubMed: 14755095]
44. Lee, T.; Hoofnagle, AN.; Resing, KA.; Ahn, NG. Protein hydrogen exchange measured by electrospray ionization mass spectrometry.. In: Celis, JE., editor. *Cell Biology: A Laboratory Handbook*. Vol. 3rd edit.. Vol. 4. Elsevier Academic Press; Burlington, MA: 2006. p. 443-449.
45. Johnson ML, Correia JJ, Yphantis DA, Halvorson HR. Analysis of data from the analytical ultracentrifuge by nonlinear least-squares techniques. *Biophys. J* 1981;36:575–588. [PubMed: 7326325]

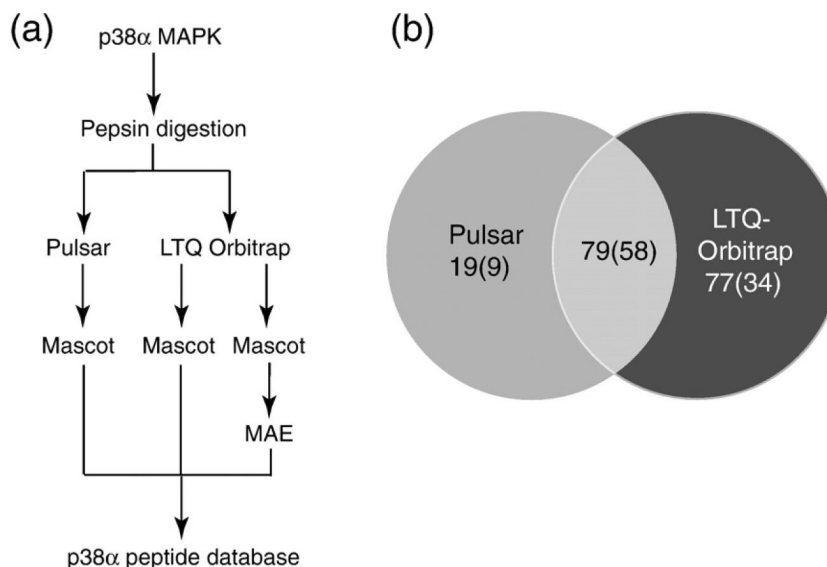


Fig. 1. Methods for LC-MS/MS data collection and analysis. (a) Experiments used to identify peptides created by pepsin digestion. Purified p38 α was proteolyzed and peptides were sequenced by LC-MS/MS on Pulsar QqTOF and LTQ-Orbitrap mass spectrometers. Data were analyzed using the Mascot search program and postprocessed using MAE in-house software, then compiled into a database of observed peptides (Supplementary Table 1). (b) Peptides identified from nine replicate LC-MS/MS runs collected on the Pulsar mass spectrometer and from three replicate runs collected on the LTQ-Orbitrap mass spectrometer. Numbers indicate total unique peptides, and parentheses indicate unique peptides matched to ions observable in HX-MS data sets.

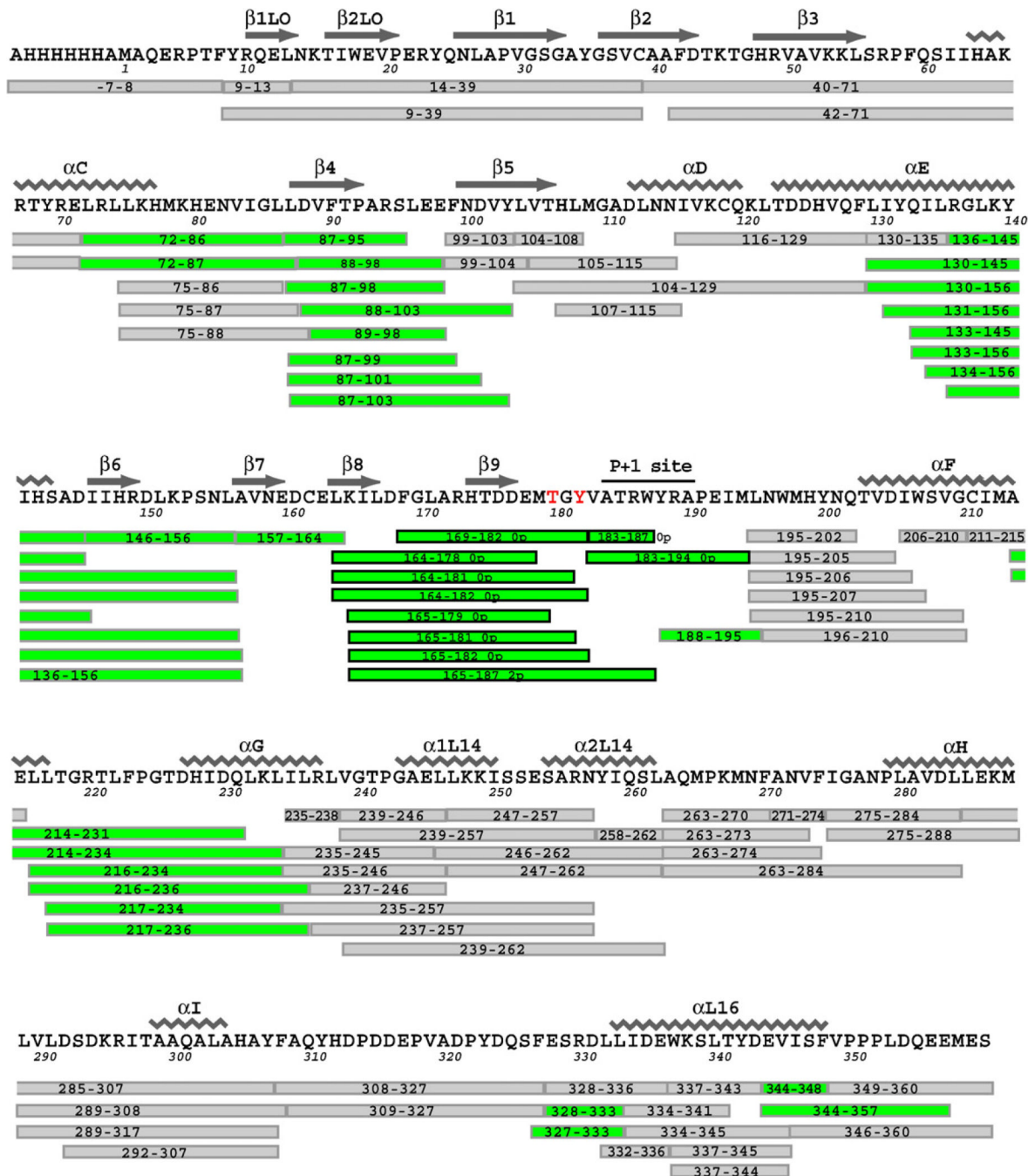


Fig. 2. Summary of HX-MS analyses of p38 α . Sequence coverage map of p38 α indicating residue numbering and secondary structures as reported.^{15,16} Observed peptides are shown as bars below the sequence and are named according to residue number. Peptides in white show cases where HX rates were unaffected by phosphorylation and activation. Peptides in green show cases where HX rates decreased significantly upon activation. All peptides were observed in both 0P and 2P forms of p38 α , except those outlined in bold, which indicate those unique to 0P-p38 α or 2P-p38 α , as indicated.

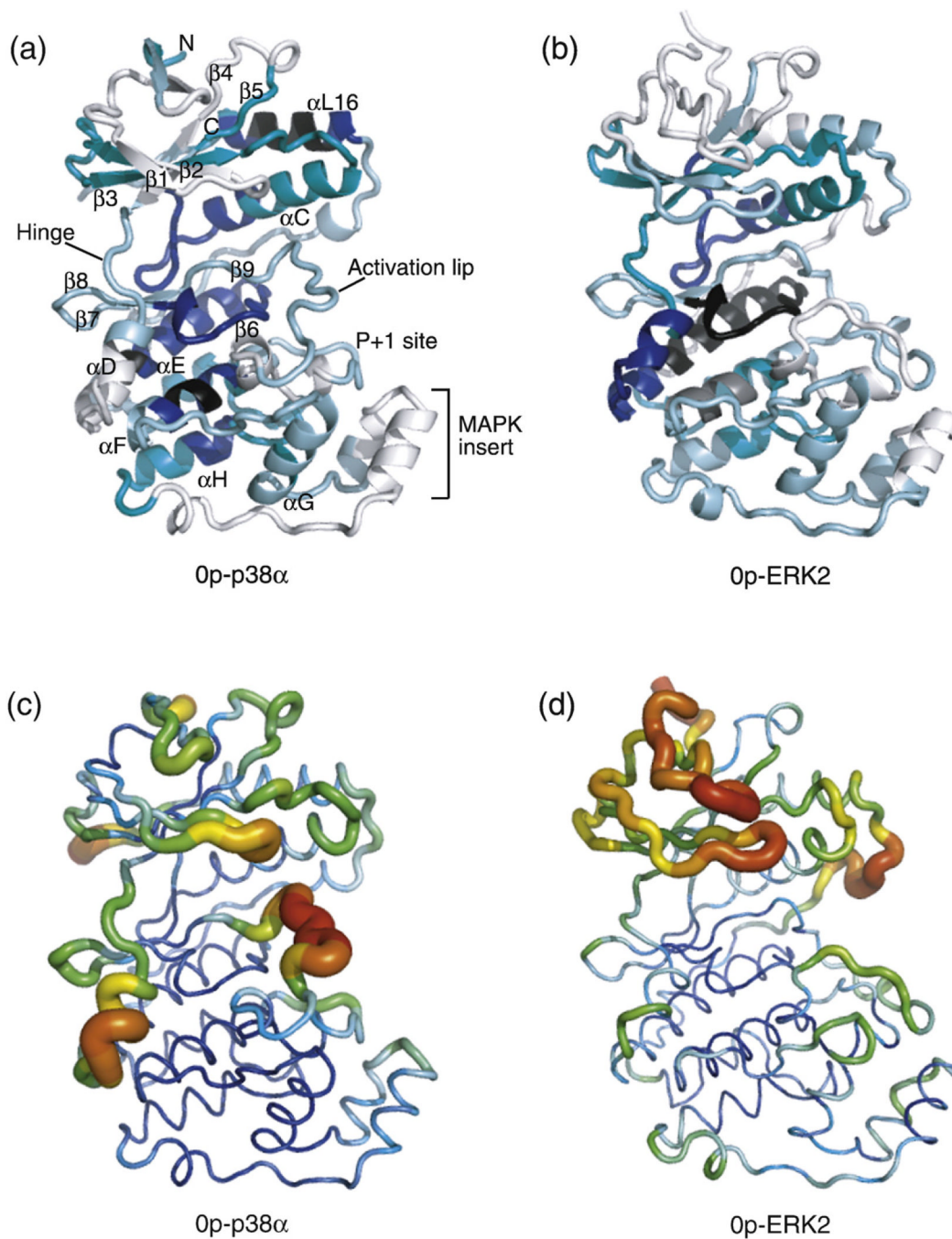


Fig. 3. Regional hydrogen–deuterium in-exchange *versus* crystallographic *B*-factors. (a) HX into OP-p38α shows extent of deuteration after 4 h, normalized for each region by the number of exchangeable amides. Colors distinguish regions deuterated to 0–20% (black), 21–40% (blue), 41–60% (teal), 61–80% (light blue), and 81–100% (white) of exchangeable amides. (b) Normalized deuterium exchange into OP-ERK2 at 4 h (data from Hoofnagle *et al.*⁷). (c and d) Crystallographic *B*-factors in p38α (1P38; Wang *et al.*¹⁵) and ERK2 (1ERK; Canagarajah *et al.*⁴). Images were generated using PyMol 0.99.

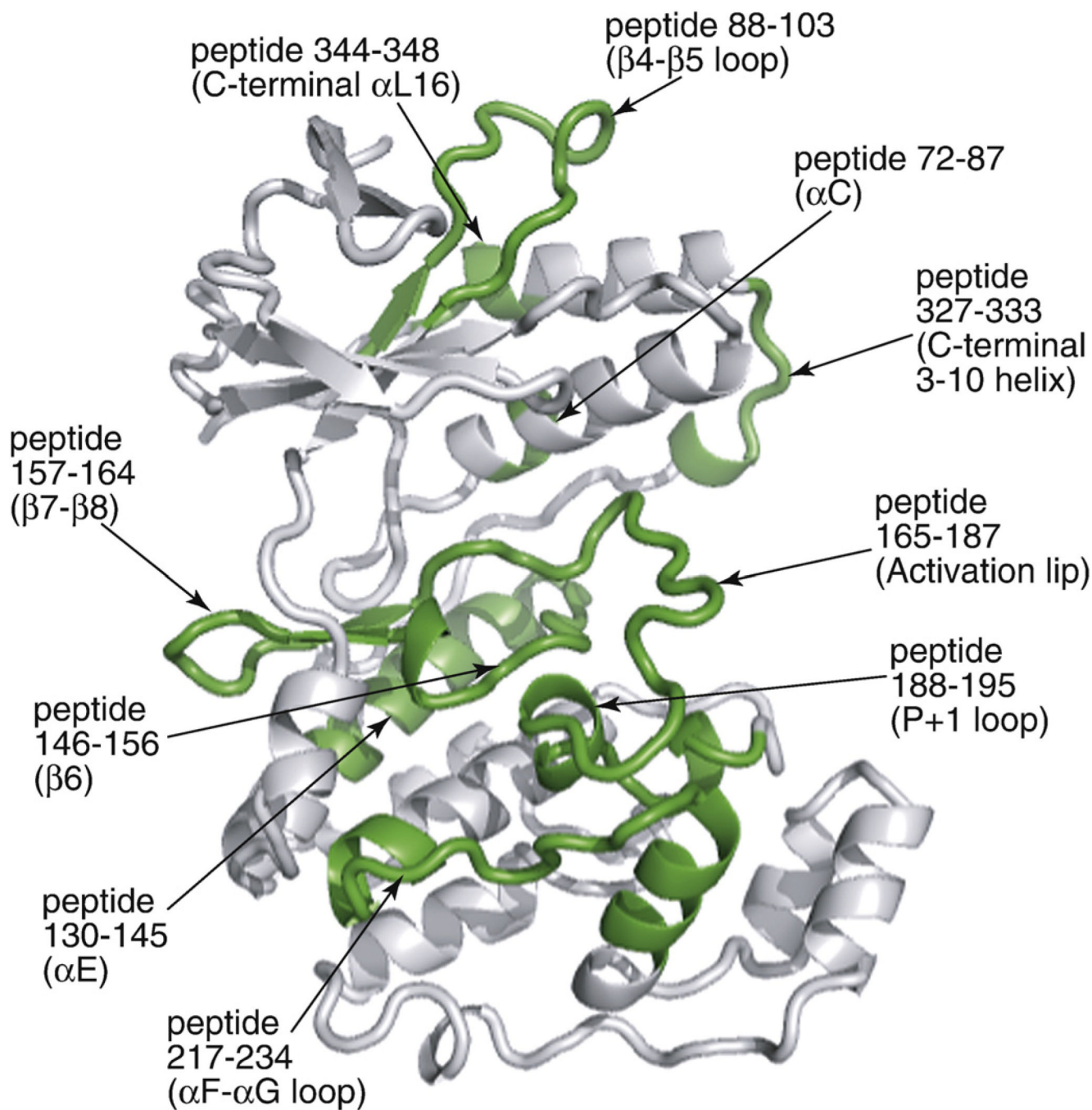


Fig. 4. Summary of HX changes induced by p38 α activation. Representative peptides show regions significantly decreased in HX upon diphosphorylation of p38 α , which are indicated in green on the main-chain ribbon structure.

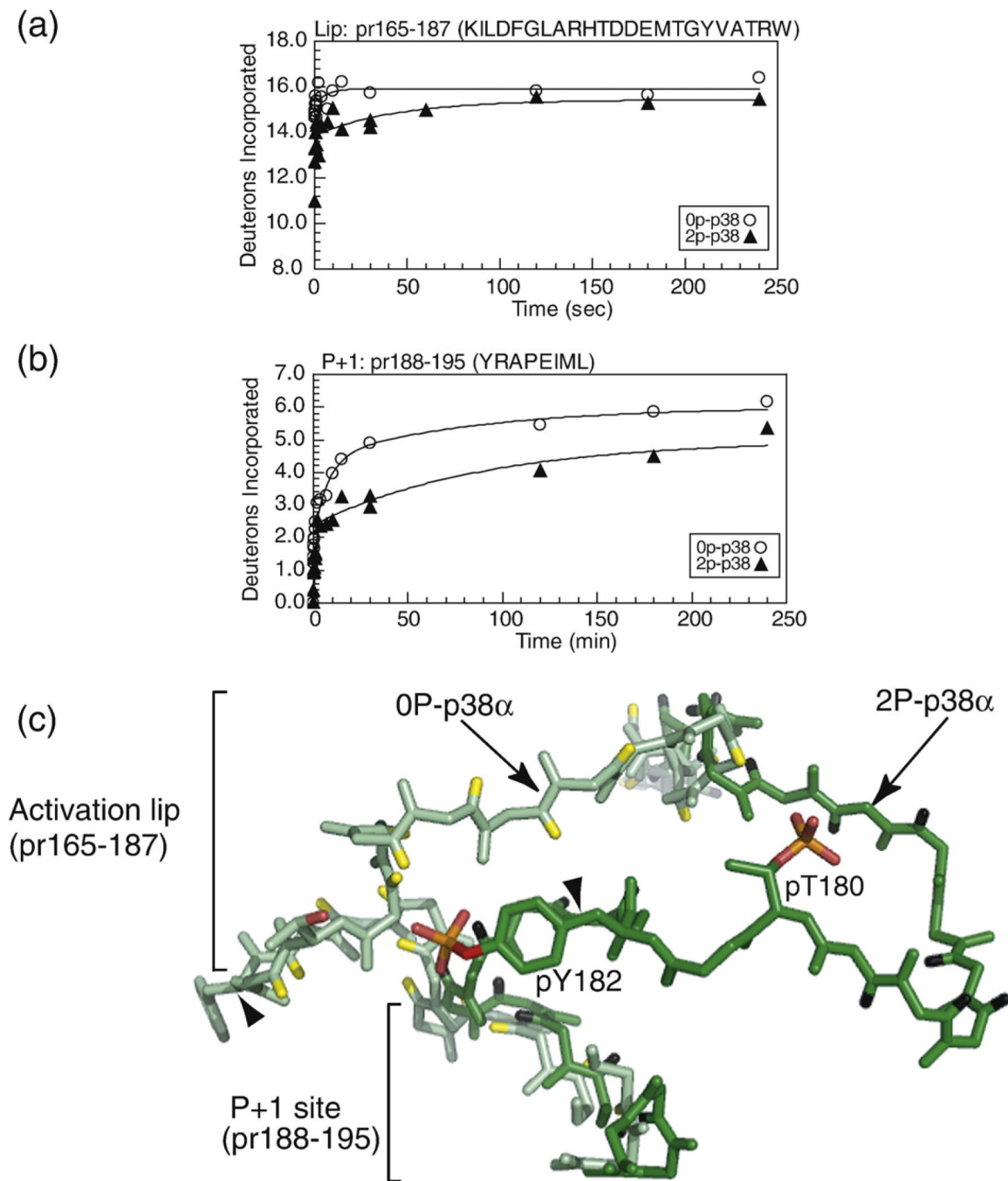


Fig. 5. Comparison of peptide HX kinetics between 0P-p38 α (○) and 2P-p38 α (▲) and associated X-ray structural differences in the activation lip and the P+1 substrate recognition site. Time courses of deuteration are shown for (a) pr165–187 in the activation lip and (b) pr188–195 in the P+1 site. In 2P-p38 α , the deuteration time course for pr165–187 is represented by a single intact peptide, whereas in 0P-p38 α , the time course represents the sum of pr165–182+pr183–187, which contains one less exchangeable amide than pr165–187 in 2P-p38 α . Nevertheless, the extent of deuteration decreases in 2P-p38 α , reflecting a significant reduction in HX. (c) C α conformation from X-ray structures of 0P-p38 α (light green; 1P38) and 2P-p38 γ (dark green; 1CM8), overlaying regions in the activation lip and the P+1 site. Amide hydrogens from

p38 α and p38 γ are represented by yellow and black sticks, respectively. Arrowheads indicate peptide cleavage sites.

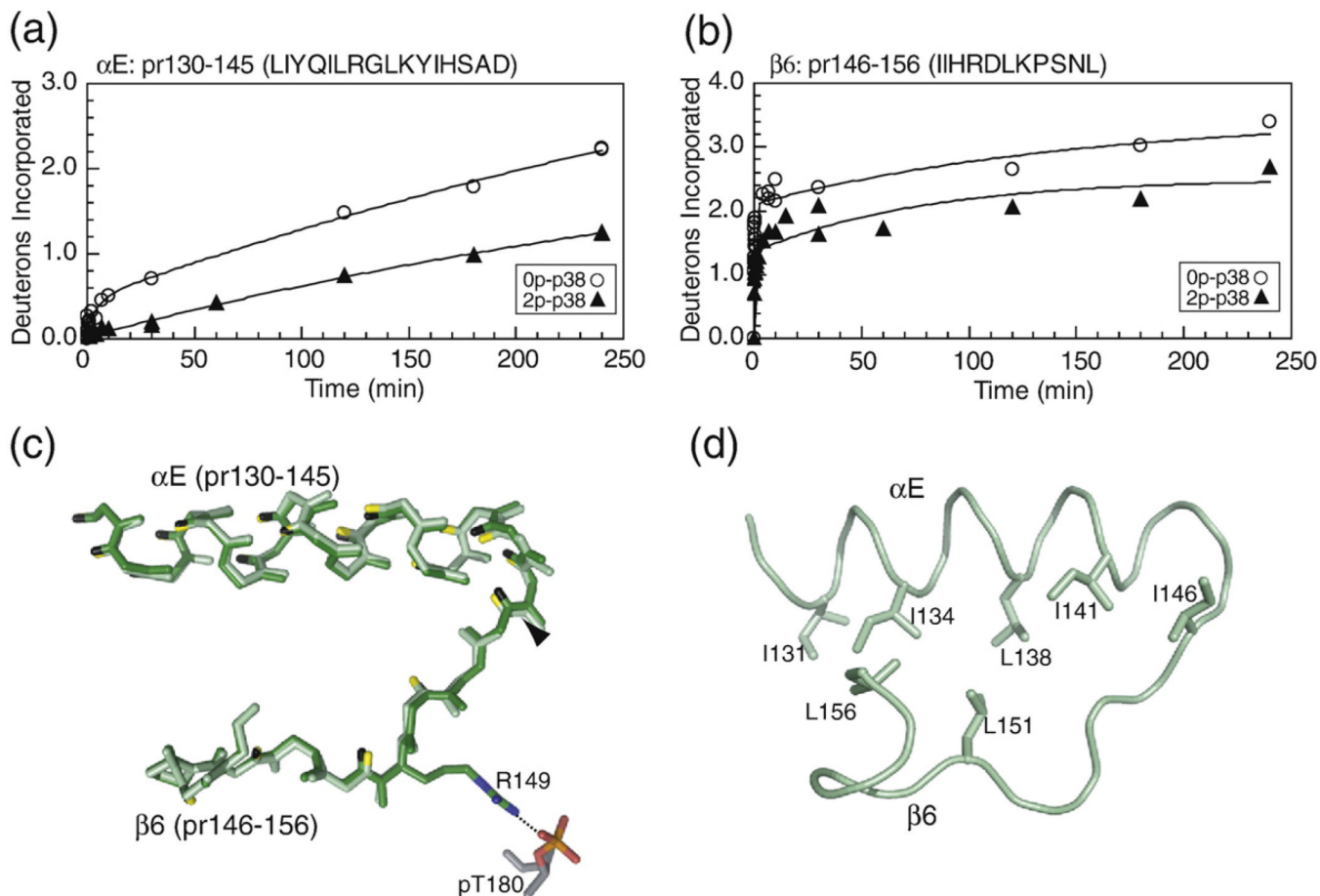


Fig. 6. HX-MS behavior and structural comparison in the C-terminal core region. Deuteration of (a) pr130–145 containing helix αE , and (b) pr146–156 containing $\beta 6$ and the catalytic base Asp150. (c) C^α structures show a similar conformation within αE between p38 α (green) and p38 γ (dark green). Residue Arg149 in $\beta 6$ forms ion pair interactions with pThr180 in the activation lip of 2P-p38 γ . Arrowheads indicate peptide cleavage sites. (d) Residue side chains between αE and $\beta 6$ suggest potential interactions for coupling between these regions.

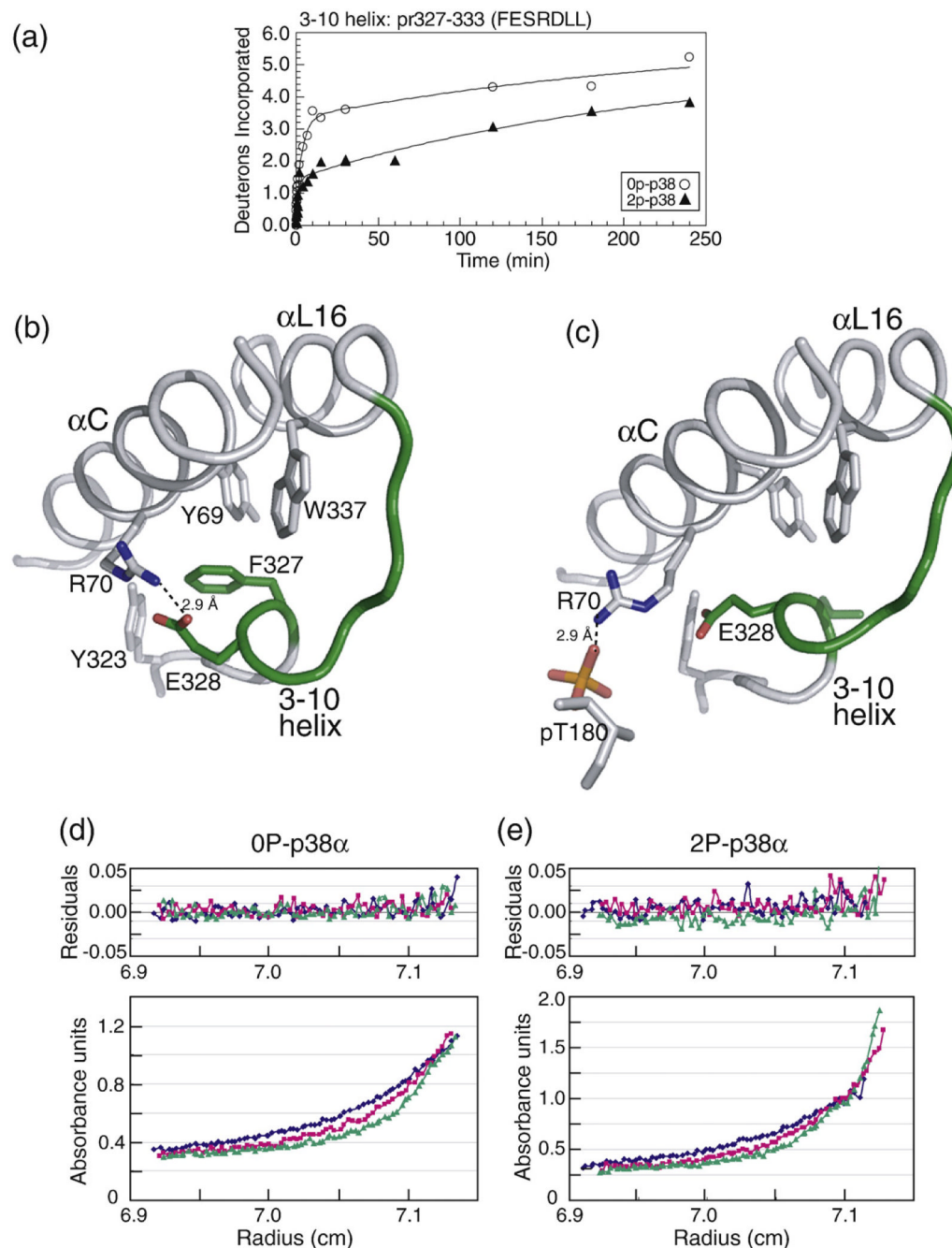


Fig. 7. HX-MS behavior and structural comparison in the C-terminal extension 3-10 helix. (a) Deuteration of pr327-333 containing the 3-10 helical turn indicates a significant reduction in HX upon p38 α activation. (b) Structure of p38 α shows side-chain interactions comprising a hydrophobic core region with side-chain connectivities between helices αC and $\alpha L16$ and the 3-10 helix. Ion pair interactions with Glu328 sequester Arg70 from interacting with activation lip residues. pr327-333 is shown in green. (c) X-ray structure of p38 α -Phe327Leu mutation (2FST; Diskin *et al.*²⁶) revealing disrupted side-chain interactions in the hydrophobic cluster and disruption of ion pair interactions between Arg70 and Glu328 (5.3 Å). Rotation of Arg70 would enable new ion pair interactions between Arg70 and pThr180 (2.9 Å), which are

observed in 2P-p38 γ . (d and e) Sedimentation equilibrium experiments carried out by analytical ultracentrifugation show that (d) 0P-p38 α and (e) 2P-p38 α are both monomeric. The bottom panel shows absorbance units *versus* radius at 20,000 rpm (blue), 24,000 rpm (red), and 28,000 rpm (green). The top panel shows residuals after fitting absorbance data to a single component model. Weighted average masses 0P-p38 α and 2P-p38 α are 40,567 Da and 42,784 Da, respectively (4–7% error).

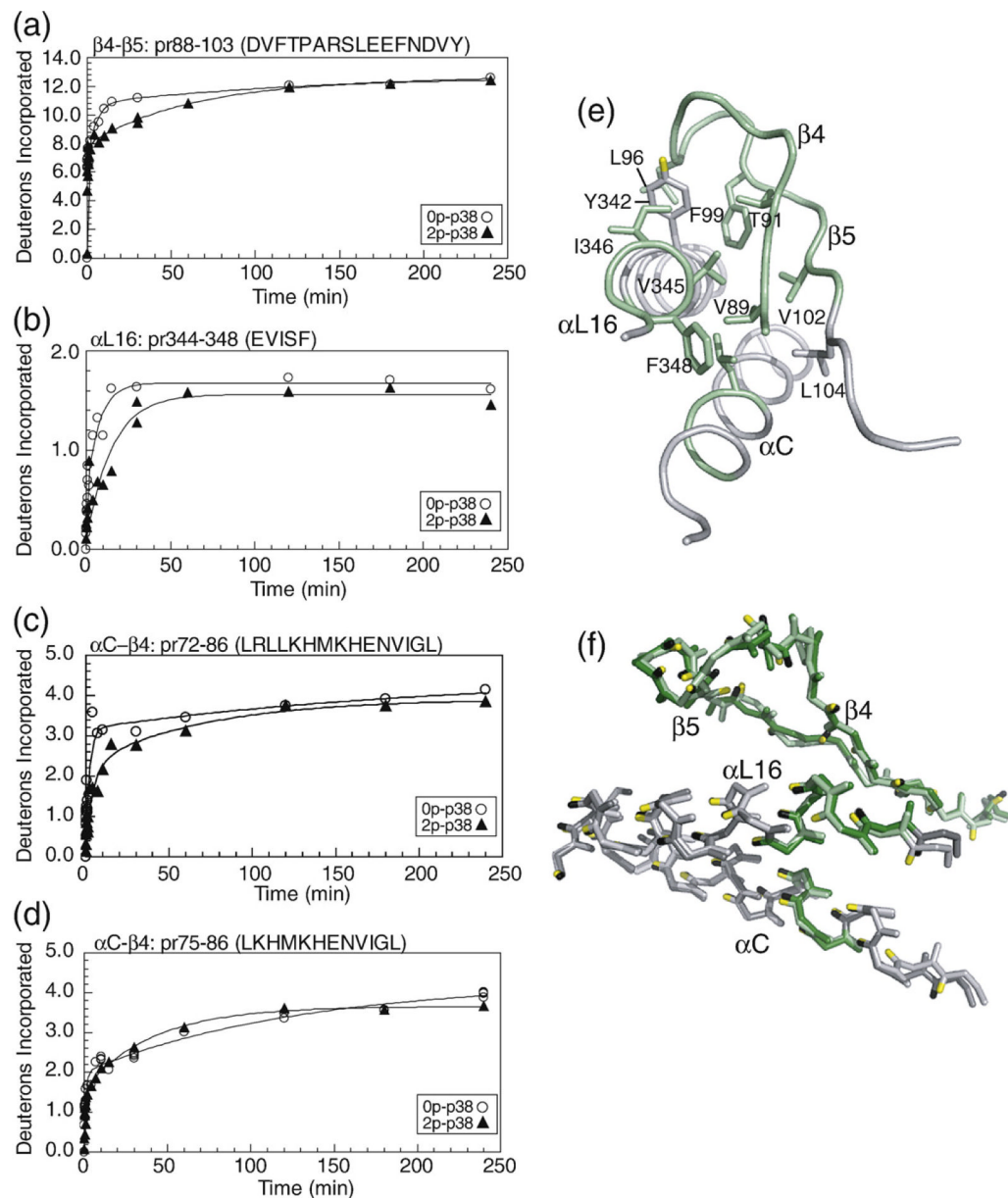


Fig. 8. HX-MS behavior and structural comparison in the N-terminal core region of p38. Deuteration of (a) pr88–103 containing $\beta 4$ – $\beta 5$ and the intervening loop, and (b) pr344–348 containing the C-terminal helix α L16. Within the α C– $\beta 4$ loop, (c) pr72–86 shows decreased HX and (d) pr75–86 shows no change, indicating that decreased HX can be localized to residues 72–75 (LRL). (e) Side-chain connectivities between $\beta 4$ – $\beta 5$, α L16, and α C, where regions with decreased HX are shown in green. (f) C^α structures closely overlap between 0P-p38 α (light green, light gray) and 2P-p38 γ (dark green, dark gray), suggesting that the changes in HX reflect alterations in protein mobility rather than in structure.

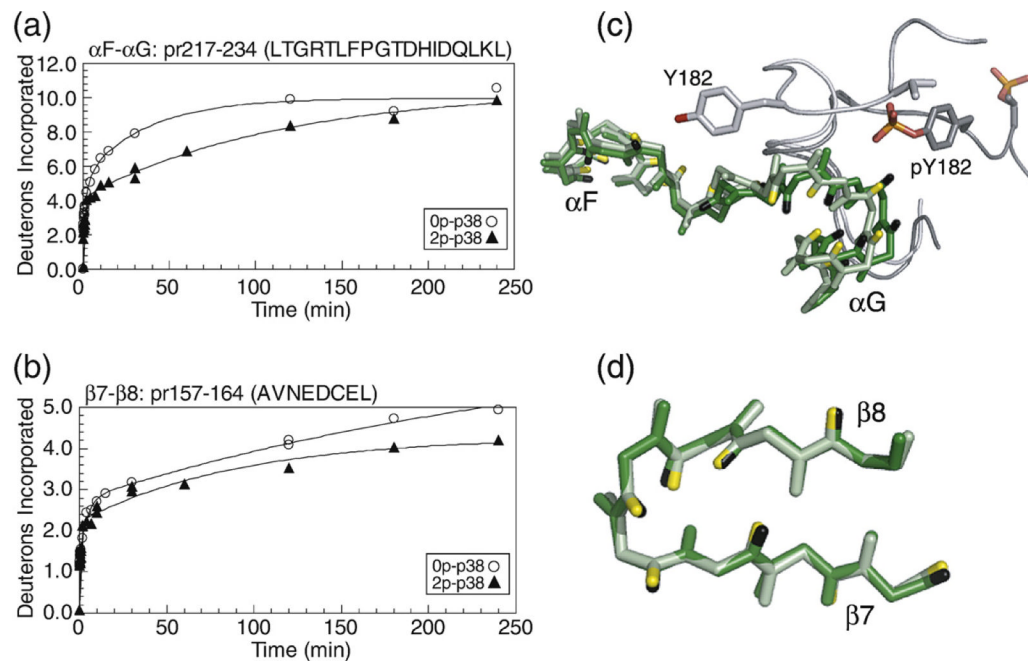


Fig. 9. HX-MS behavior and structural comparisons within substrate-binding regions. Time courses of deuteration for (a) pr217–234 in the αF – αG loop, which comprises an extended substrate-binding groove, and (b) pr157–164 in the $\beta 7$ – $\beta 8$ loop, which comprises part of the DEJL docking motif-binding site. (c and d) C^α structures of 0P-p38 α (light green) and 2P-p38 γ (dark green), overlaying regions in the (c) αF – αG loop and the (d) $\beta 7$ – $\beta 8$ loop.

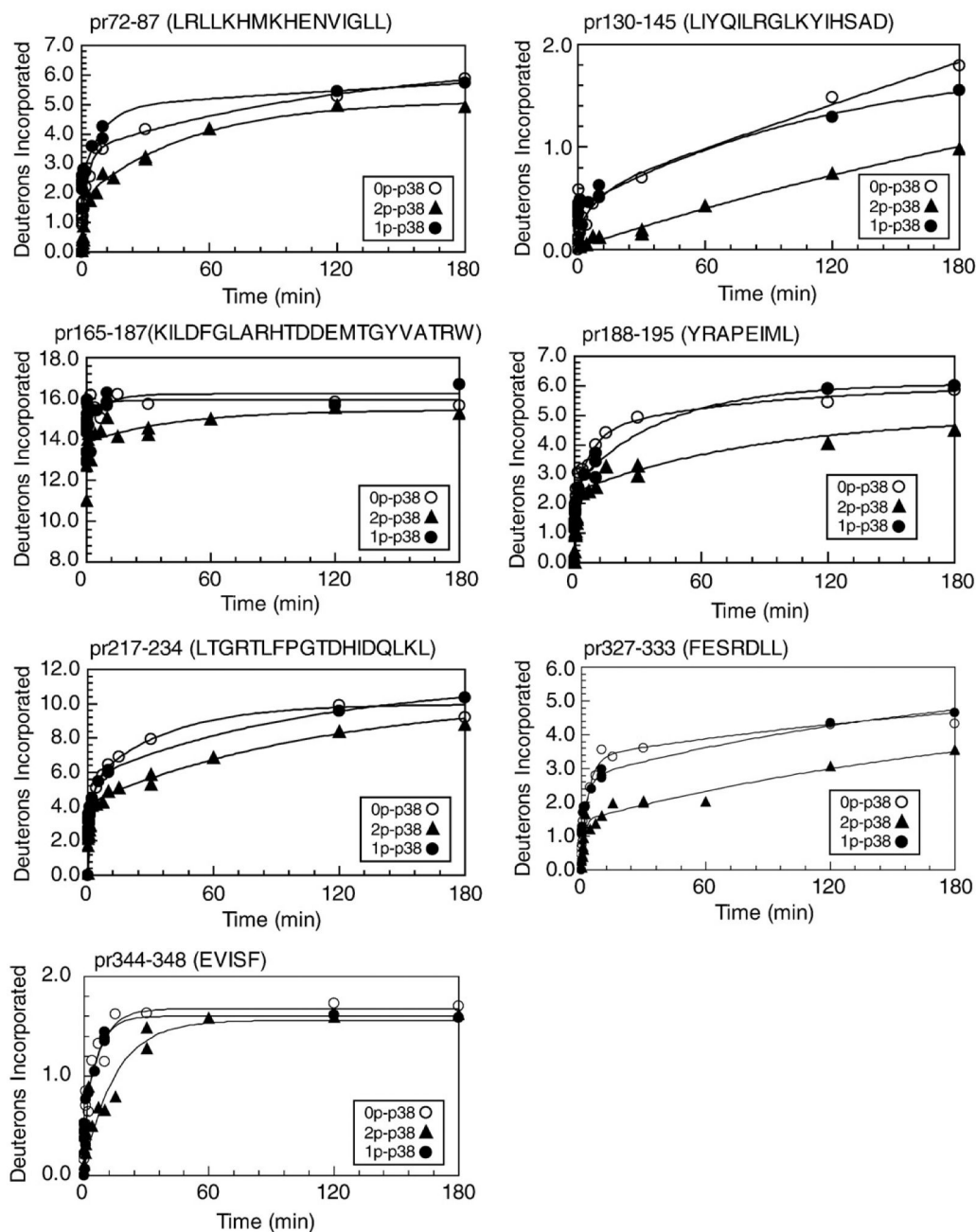


Fig. 10. HX-MS behavior of monophosphorylated p38 α . Deuteration time courses of peptides from p38 α monophosphorylated at Tyr182 (\bullet) are superimposed on time courses of 0P-p38 α (\circ) and 2P-p38 α (\blacktriangle). In 1P-p38 α , deuteration time courses of those peptides that significantly decreased in 2P-p38 α more closely resemble those of 0P-p38 α .

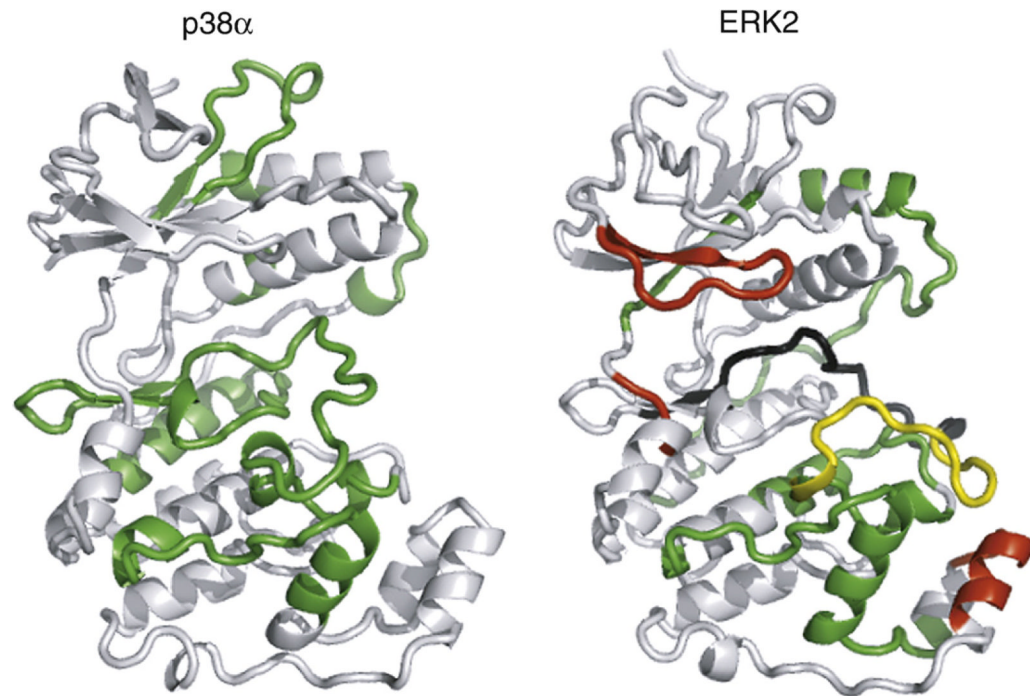


Fig. 11.

Comparison of activation-induced changes in HX-MS in MAPKs. Regulated HX in p38 α from this study is compared to that of ERK2 from Hoofnagle *et al.*⁷ Green indicates regions where HX decreases upon kinase activation, and red indicates regions where HX increases upon kinase activation. Yellow indicates the activation lip, where both increases and decreases in HX rates could be observed, ascribed to conformational remodeling upon activation. Black indicates a region where 0P- and 2P-ERK2 could not be compared due to insufficient peptide overlap. The result shows that conservation of sequence and tertiary structure does not lead to conservation of regulated conformational mobility.

Table 1

Peptides recovered from LC-MS/MS experiments and sequence coverage

Instrument (analysis method)	Total peptide IDs				Peptides matching the HX-MS data set			
	Number of runs	Unique peptides	Full sequence coverage (%)	Unique peptides	Coverage of exchangeable amides (%)	Minimum peptides covering sequence	Peptides with overlapping sequence	
Pulsar QqTOF (Mascot)	1	39	77	30	64	21	9	
	3	77	88	45	81	24	21	
	9	98	99	67	95	28	39	
LTQ-Orbitrap (Mascot)	1	95	86	61	72	22	39	
	3	110	86	68	81	23	45	
LTQ-Orbitrap (Mascot+MAE)	1	129	90	78	75	24	54	
	3	151	93	87	90	27	60	
LTQ-Orbitrap (Total IDs, Pulsar +LTQ-Orbitrap IDs)	1	132	96	81	80	26	55	
	3	156	99	92	95	29	63	
	12	175	100	101	98	29	72	

The summary of results for unique peptide sequences, with full data set, is presented in Supplementary Table 1.